Pergamon

Continental Shelf Research, Vol. 16, No. 1, pp. 101–130. 1996

0278–4343/96 $9.50 + 0.00

23563 0278–4343(95)E00005–4

Presentation of a family of turbulence closure models for stratified shallow water flows and preliminary application to the Rhine outflow region

PATRICK J. LUYTEN,*† ERIC DELEERSNIJDER,‡ JOSÉ OZER† and KEVIN G. RUDDICK†

(*Received* 6 *January* 1994; *in revised form* 17 *November* 1994; *accepted* 12 *December* 1994)

Abstract—Three turbulence closure schemes, designed for stratified shallow water flows, are presented. They are based upon k-ε theory and use respectively two, one or zero transport equations for turbulent variables. The models are first tested on the evolution of a wind-driven turbulent layer in a stratified fluid. The results are at least qualitatively in agreement with observational and experimental data. A discussion is given about the existence of self-similar solutions. The models are compared next with the observational data of the Rhine outflow area. The periodic variation in the density structure, forced by wind and tides and which is clearly visible in the data, is predicted by the model. A physical interpretation of the model results is given in the absence of wind forcing. The effects of estuarine circulation, tidal straining and mixing on the development or breakdown of stratification are well represented by the model calculations.

1. INTRODUCTION

It is widely acknowledged that the parameterization of vertical diffusion of momentum and scalar quantities (heat, salinity) often represents a crucial weakness in the current generation of shelf sea circulation models (Gesamp, 1991), especially for regions where thermal or haline stratification occur: vertical diffusion by turbulent fluctuations is both rarely negligible, since in shallow water bottom and surface friction often penetrate the whole water column, and is difficult to describe mathematically because it is highly non-linear. In the northern North Sea thermal stratification occurs in summer, where the tendency of solar radiation to stratify the surface layer is stronger than mixing induced by wind and tide (Simpson and Hunter, 1974). Haline stratification may occur in the Region Of Freshwater Influence (ROFI) of major rivers, where the tendency to stratify is here provided by freshwater run-off. For example, much of the Dutch coastal zone may become stratified by the discharge of the river Rhine (van der Giessen *et al.*, 1990). Observations by

*Author to whom all correspondence should be addressed.
†Management Unit of Mathematical Models of the North Sea and Scheldt Estuary (MUMM), 100 Gulledelle, B-1200 Brussels, Belgium.
‡Institut d'Astronomie et de Géophysique G. Lemaître, Université Catholique de Louvain, Chemin du Cyclotron 2, B-1348 Louvain-La-Neuve, Belgium.

Simpson *et al.* (1993) indicate significant semi-monthly and semi-diurnal variability in this stratification. A similar pattern has been observed in Liverpool Bay (Simpson *et al.*, 1991).

For computational efficiency, and perhaps for program simplicity and reliability, most models do not resolve turbulent fluctuations but parameterize their effect through a turbulence closure scheme. Each quantity (momentum, temperature, salinity) is split into a mean and a fluctuating part. Although exact equations exist for those mean quantities, they contain unknown second-order correlations between the fluctuating components of momentum and the buoyancy, i.e. the Reynolds shear stresses and the turbulent fluxes of scalar quantities (temperature, salinity). Closure assumptions therefore need to be introduced. The turbulent fluxes can in principle be determined as the solutions of at least 10 transport equations after making model assumptions for the higher order correlations. Since this involves a considerable amount of computing time, the equations are usually reduced to an algebraic system. Examples of such simplifications are proposed by Mellor and Yamada (1974, 1982), or Gibson and Launder (1976). For a review see Rodi (1984). The parameterizations introduced in the original system of equations require the determination of two additional turbulent quantities. A commonly used variable is the turbulent kinetic energy k for which a transport equation can be derived. Less agreement exists about an optimum choice for the second parameter. Mellor and Yamada (1982) suggest to use the turbulent length scale l which can be determined from a separate transport equation for the product kl (Mellor and Herring, 1973), or prescribed algebraically. For shallow water flows the boundary layer approximation can be applied so that the algebraic system for the turbulent fluxes can be further simplified. The expressions for the vertical fluxes of momentum or salinity (temperature) then reduce to their known forms as the product of an eddy viscosity or diffusivity times the vertical gradient of momentum or salinity (temperature). Additional improvements are considered by Galperin *et al.* (1988).

Turbulence energy models using $k - l$ (or $k - kl$) theory have been incorporated into circulation models for the ocean and shelf seas by e.g. Blumberg and Mellor (1987), Oey and Chen (1992), Rosati and Miyakoda (1988), Davies and Jones (1990), Johns *et al.* (1992). An alternative theory, which uses the dissipation rate ε of turbulent energy instead of the mixing length scale, is advocated by Launder and Spalding (1974), Rodi (1987). The prime difference with the $k - l$ version is the use of a modelled transport equation for ε. It has the advantage that it does not require a wall proximity function to give the correct behaviour near a solid wall. A parameterized ε-equation can be derived from the more general exact vorticity equation (Tennekens and Lumley, 1972). Applications of $k - \varepsilon$ theories to circulation problems in shelf and coastal seas are discussed by e.g. Kochergin (1987), Baumert and Radach (1992), Baum and Caponi (1992).

This paper deals with the presentation and testing of three turbulence closure schemes, denoted by KEPS2, KEPS1, KEPS0. They differ by the number of transport equations used for turbulent variables and are based upon $k - \varepsilon$ theory. The turbulent fluxes are expressed in terms of the local values of k, ε and the local gradient of the corresponding mean quantity using the boundary layer approximation and the assumption that the Reynolds stresses are in a state of near isotropy (Mellor and Yamada, 1982; Galperin *et al.*, 1988). The transition layer where turbulence decays into a field of internal waves (see e.g. Hopfinger, 1987) is taken into account by imposing limiting conditions on the turbulent variables. The KEPS2 model uses transport equations for k and ε. Since the latter equation involves more model assumptions, it is replaced by an algebraic length scale prescription in the second model (KEPS1). The k-equation is also reduced to an algebraic relation in the

third model (KEPS0) using the assumption of local equilibrium between production and dissipation of turbulent energy. This model is similar to the Mellor–Yamada level 2 scheme. The KEPS0 model has the advantage that it requires practically the same amount of computing time as simpler eddy viscosity parameterizations, such as the relations of Munk and Anderson (1948) while it is derived on a more physical basis. On the other hand, it appeared that the level 2 scheme is sensitive to numerical instabilities depending on time step and vertical grid spacing (Frey, 1991). The models are first tested on the evolution of a turbulent layer driven by a constant wind stress. This simple test case allows a direct comparison with observational and laboratory data and with the analytical theory. To validate their performance in coastal zones with a strong stratification they are also compared with the observational data of the Rhine outflow area.

2. MODEL EQUATIONS

2.1 *General theory*

A rotating Cartesian coordinate system is used with the origin at the sea surface and the z-axis directed upwards along the vertical. The turbulent equations of motion, using the Boussinesq approximation, are given by

$$\frac{\partial U_i}{\partial t} + U_k \frac{\partial U_i}{\partial x_k} - \varepsilon_{ik3} f U_k = -\frac{\partial P}{\partial x_i} + b\delta_{i3} + \nu \frac{\partial^2 U_i}{\partial x_k^2} - \frac{\partial}{\partial x_k} \langle u_i u_k \rangle \tag{1}$$

$$\frac{\partial U_i}{\partial x_i} = 0 \tag{2}$$

where U_i, u_i represent respectively the ensemble mean and fluctuation velocity, f the Coriolis frequency, ν the coefficient of molecular kinematic viscosity and $\langle u_i u_j \rangle$ the turbulent momentum fluxes, using angle brackets for ensemble averages of turbulent quantities. The reduced pressure and the buoyancy are defined by

$$P = \frac{p}{\rho_0} + gz \tag{3}$$

$$b = -g \frac{\rho - \rho_0}{\rho_0} \tag{4}$$

where p denotes the pressure, g the acceleration of gravity, ρ the density and ρ_0 a reference density. The density (buoyancy) is related to the temperature T and the salinity S through an equation of state. For simplicity, it is assumed that the transport equations for T and S can be combined into a single equation for the buoyancy, given by

$$\frac{\partial b}{\partial t} + U_i \frac{\partial b}{\partial x_i} = \lambda_b \frac{\partial^2 b}{\partial x_i^2} - \frac{\partial}{\partial x_i} \langle u_i \beta \rangle \tag{5}$$

where λ_b is the molecular diffusion coefficient for the buoyancy, β the fluctuation buoyancy and $\langle u_i \beta \rangle$ are the turbulent buoyancy fluxes. The last terms on the right-hand side of equations (1) and (5) can be decomposed into a horizontal and a vertical diffusion term. The former terms are neglected in the present study.

The vertical fluxes of momentum and buoyancy are written in the form

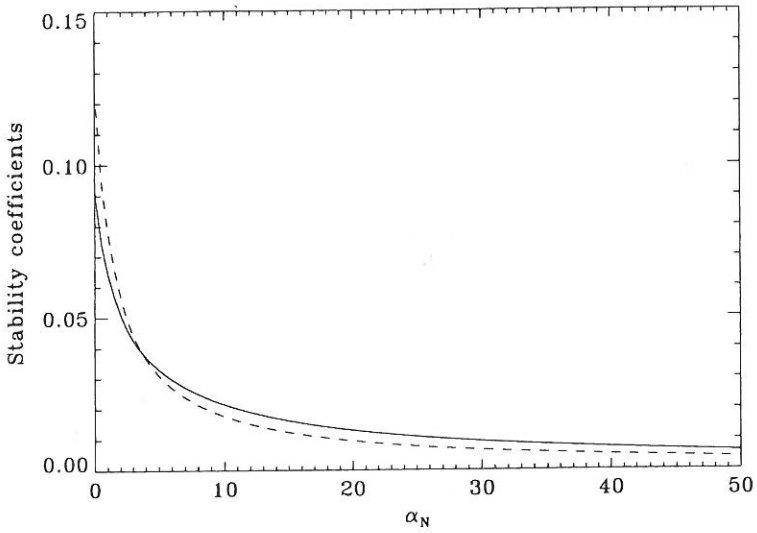

Fig. 1. Variation of the stability coefficients S_u (solid) and S_b (dashes) as function of α_N in the case of stable stratification.

$$-\langle uw\rangle = \nu_T U_z, \qquad -\langle vw\rangle = \nu_T V_z, \qquad -\langle w\beta\rangle = \lambda_T b_z \tag{6}$$

where the subscript z denotes a derivative with respect to the vertical coordinate. In the $k-\varepsilon$ formulation the eddy coefficients take the form

$$\nu_T = S_u k^2/\varepsilon, \qquad \lambda_T = S_b k^2/\varepsilon \tag{7}$$

where k represents the turbulent kinetic energy and ε the dissipation of k by molecular viscosity. The stability coefficients S_u and S_b are expressed as function of stratification in the following way

$$S_u = \frac{0.091 + 0.023\alpha_N}{1 + 0.714\alpha_N + 0.067\alpha_N^2} \tag{8}$$

$$S_b = \frac{0.125}{1 + 0.603\alpha_N} \tag{9}$$

where

$$\alpha_N = \frac{k^2}{\varepsilon^2} N^2 \tag{10}$$

and N is the Brunt–Väisälä frequency, defined by $N^2 = \partial b/\partial z$. Details of the calculations which are based upon the theory described in Rodi (1984), the local equilibrium assumption and the boundary layer approximation are described in the Appendix. The reduction of turbulence in the presence of a stable density gradient can be seen in Fig. 1 which shows the evolution of S_u and S_b as function of α_N. To close the system of equations suitable expressions must be derived for the turbulent quantities k and ε. The following

three models, whose complexity depends on the number of transport equations used for either k or ε, will be considered:

(1) transport equations for k and ε (KEPS2);
(2) transport equation for k, algebraic expression for ε (KEPS1);
(3) algebraic expressions for k and ε (KEPS0).

The transport equations generally include source and sink terms and terms representing advection and diffusion.

2.2 *KEPS2-model*

A transport equation for the turbulent energy k can be derived in the usual way by adding the diagonal components of equations (A1) for the turbulent fluxes $\langle u_i u_j \rangle$. If one assumes gradient diffusion of the form

$$-\langle u_i k \rangle = \nu_T \frac{\partial k}{\partial x_i} \Big/ \sigma_k \tag{11}$$

the resulting equation takes the form

$$\frac{\partial k}{\partial t} + U_i \frac{\partial k}{\partial x_i} = \frac{\partial}{\partial x_i}\left(\frac{\nu_T}{\sigma_k}\frac{\partial k}{\partial x_i}\right) + P_s + G - \varepsilon \tag{12}$$

where

$$P_s = \nu_T(U_z^2 + V_z^2), \qquad G = -\lambda_T b_z. \tag{13}$$

The parameterized equation for the turbulent dissipation is given by (Launder and Spalding, 1974; Rodi, 1984):

$$\frac{\partial \varepsilon}{\partial t} + U_i \frac{\partial \varepsilon}{\partial x_i} = \frac{\partial}{\partial x_i}\left(\frac{\nu_T}{\sigma_\varepsilon}\frac{\partial \varepsilon}{\partial x_i}\right) + c_{1\varepsilon}\frac{\varepsilon}{k}(P_s + c_{3\varepsilon}G) - c_{2\varepsilon}\frac{\varepsilon^2}{k}. \tag{14}$$

The following values are adopted for four of the empirical parameters (Launder and Spalding, 1974):

$$(c_{1\varepsilon}, c_{2\varepsilon}, \sigma_k, \sigma_\varepsilon) = (1.51, 1.92, 1.0, 1.3). \tag{15}$$

The parameter $c_{1\varepsilon}$ is determined from the relation

$$c_{1\varepsilon} = c_{2\varepsilon} - \frac{\kappa^2}{\sqrt{c_\mu}\sigma_\varepsilon} \tag{16}$$

valid for a near-wall local equilibrium flow in the absence of stratification where $\kappa = 0.4$ is von Karman's constant and

$$c_\mu = S_u(0) = 0.091. \tag{17}$$

Following Rodi (1987), $c_{3\varepsilon}$ takes the value of 1 in the case of an unstable stratification ($N^2 < 0$) and 0.2 for stably stratified flows.

2.3. *KEPS1-model*

The KEPS1-model is a simplified version of the previous one. Instead of solving a transport equation for ε which involves more model assumptions than the corresponding equation for k, the turbulent dissipation is modelled according to

$$\varepsilon = \varepsilon_0 \frac{k^{3/2}}{l} \tag{18}$$

where ε_0 is a constant and l a prescribed algebraic turbulent length scale. The parameter ε_0 is determined for an equilibrium neutral flow near a wall where l is equal to κ times the distance to the wall. This gives

$$\varepsilon_0 = c_\mu^{3/4} = 0.166. \tag{19}$$

Various expressions exist in the literature for the mixing length l. Two formulations will be considered in the test cases, discussed below. The first is the Blackadar (1962) formula

$$l = \frac{\kappa z_*}{\kappa z_*/l_0 + 1} \tag{20}$$

where z_* represents either the distance to the surface or to the bottom so that $l \to l_0$ sufficiently far from the boundary. A commonly used value for l_0 is the one proposed by Mellor and Yamada (1974):

$$l_0 = \gamma \int_0^H k^{1/2} z_* \, dz_* \Big/ \int_0^H k^{1/2} \, dz_* \tag{21}$$

where H is the total water depth and γ a constant situated in the range 0.1–0.4. The Blackadar formula depends explicitly on turbulence energy via (21), but seems less appropriate when two boundary layers are present (at the surface and at the bottom). In that case the following simpler formulation, proposed by e.g. Robert and Ouellet (1987) and used by Simpson and Sharples (1992) in their simulations for Liverpool Bay, will be used:

$$l = \kappa z_* (1 - z_*/H)^{1/2} \tag{22}$$

where z_* is the distance from the bottom.

2.4. *KEPS0-model*

Further simplification can be obtained by neglecting the material derivative and diffusion term in the k-equation so that the production of turbulent kinetic energy is always balanced by dissipation, i.e. $P_s + G = \varepsilon$. Using (13), (7) and (A13) one readily verifies that

$$\alpha_M S_u - \alpha_N S_b = 1. \tag{23}$$

Substituting expressions (8) and (9) for S_u and S_b into (23) and taking account of the definitions of α_M and α_N the following relation is obtained

$$\frac{\varepsilon^4}{k^4} + (d_1 N^2 + d_2 M^2) \frac{\varepsilon^2}{k^2} + d_3 M^2 N^2 + d_4 N^4 = 0 \tag{24}$$

where

$$(d_1, d_2, d_3, d_4) = (0.839, -0.091, -0.023, 0.081) \tag{25}$$

and $M^2 = (\partial U/\partial z)^2 + (\partial V/\partial z)^2$ is the squared shear frequency. The solution for ε^2/k^2 is given by the largest of the two roots of (24). It can then be shown that

(1) ε^2/k^2 is real;
(2) ε^2/k^2, S_u, S_b and α_M are positive when the Richardson number $Ri = N^2/M^2 < Ri_c = 0.28$ while turbulence ceases when $Ri > Ri_c$;
(3) α_N and N^2 have the same sign.

The turbulent variables k and ε are determined from the algebraic expressions (24) and (18) where l is prescribed either from (20) and (21) or (22).

Miles (1961) and Howard (1961) showed that $Ri > 0.25$ is a sufficient condition for shear flow stability. This value has also been confirmed by measurements in the ocean (Kundu and Beardsley, 1991). Although Ri_c has a somewhat larger value than this critical Richardson number, it is explained below that turbulence already decays at smaller values of Ri.

2.5 *Limiting conditions*

Evidence has been found that the size of turbulent eddies is limited in the presence of a stable stratification. This is supported by observational data (Dillon, 1982; Crawford, 1986) and by laboratory measurements (Dickey and Mellor, 1980; Stillinger *et al.*, 1983; Itsweire *et al.*, 1986). A detailed discussion can be found in the review papers by Hopfinger (1987) and Gregg (1987). The problem can be defined in terms of the Ozmidov scale L_R and the overturn length scale L_t, defined by

$$L_R = (\varepsilon/N^3)^{1/2}, \qquad L_t = -\langle\beta^2\rangle^{1/2}/N^2. \tag{26}$$

The data indicate that turbulence can only exist when $L_t/L_R \leq 0.8$, although higher values are not excluded (Galperin *et al.*, 1989). When the ratio L_t/L_R attains its critical value, the largest turbulent eddies decay into internal waves.

The analysis has the following implications on the model equations. Using (26), (A12), (6), (7) and (A13) one finds that

$$\frac{L_t}{L_R} = (2c_{3\beta})^{1/2} S_b^{1/2} \alpha_N^{3/4}. \tag{27}$$

The right-hand side of (27) increases while S_u and S_b [see equations (8) and (9)] decrease as a function of α_N. Those quantities are accordingly limited by conditions of the form $\alpha_N \leq \alpha_{Nc}$, $S_u \geq S_{uc}$, $S_b \geq S_{bc}$. From the definition of α_N and equation (18) it follows that

$$\varepsilon \geq \varepsilon_{\min} = \alpha_{Nc}^{-1/2} kN \tag{28}$$

$$\frac{Nl}{(2k)^{1/2}} \leq (\alpha_{Nc}/2)^{1/2} \varepsilon_0 = K. \tag{29}$$

Galperin *et al.* (1989) suggest that $0.3 \leq K \leq 0.6$. Its value is related to the critical values of the Richardson number Ri and the flux Richardson number $R_f = -G/P$. Using (13) and (7)–(10) it is possible to express Ri and R_f as a function of α_N (or K) and the

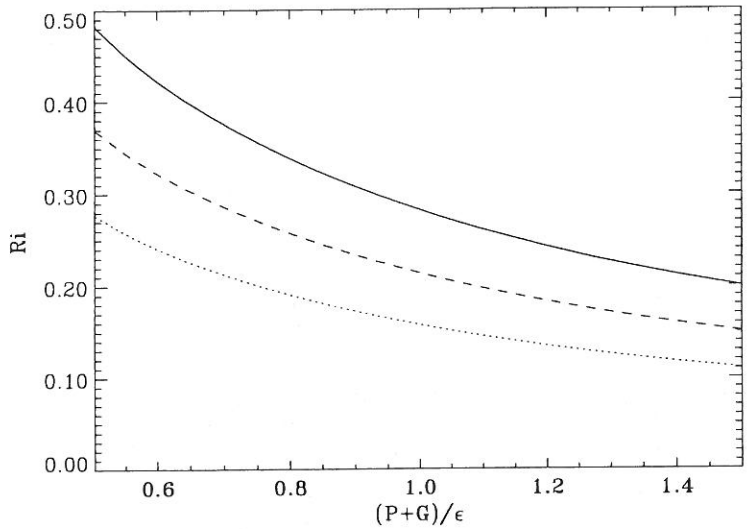

Fig. 2. Variation of the Richardson number as function of the ratio of total production to dissipation of turbulence energy using a limiting condition of the form (29): $K = \infty$ (solid), $K = 0.5$ (dashes), $K = 0.3$ (dots).

ratio $(P_s + G)/\varepsilon$. Figure 2 shows the variation of Ri as a function of this ratio for different values of K. It can be seen that lowering the value of K, which is equivalent to decreasing the value of the ratio L_t/L_R, reduces the Richardson number and therefore increases the stabilizing effect of stratification on turbulence. Following Galperin *et al.* (1989) the value of $K = 0.53$ is adopted. This implies that $Ri_c = 0.22$ and $R_{fc} = 0.16$, assuming equilibrium between production and dissipation of turbulence, i.e. $P_s + G = \varepsilon$, at the critical layer. The value of R_{fc} is close to 0.15, proposed by Osborn (1980). It is also well situated between the observed oceanic bounds $0.11 \leqslant R_{fc} \leqslant 0.32$ (Moum *et al.*, 1989) and $0.11 \leqslant R_{fc} \leqslant 0.26$ (Oakey, 1982). With this value for K one finds that

$$\alpha_{Nc} = 20.4, \qquad \varepsilon_{\min} = 0.22kN. \tag{30}$$

In the case of an unstable stratification a lower bound for α_N is imposed by requiring that α_M, defined by (A13), remains positive, when the assumption is made that $P_s + G = \varepsilon$. The derivation is analogous to the one described in Galperin *et al.* (1988). Using (23), (8) and (9) α_M can be expressed as a function of α_N and remains positive provided that

$$\alpha_N \geqslant -1.37. \tag{31}$$

If (31) is satisfied, it can in addition be shown from (8) and (9) that S_u and S_b always remain finite and positive.

2.6 *Boundary conditions and method of solution*

For the test cases, discussed below, the momentum and turbulence equations are solved without the horizontal diffusion and advection terms. The equations of motion accordingly reduce to

$$\frac{\partial U}{\partial t} - fV = -\frac{1}{\rho}\frac{\partial P}{\partial x} + \frac{\partial}{\partial z}\left((\nu_T + \nu)\frac{\partial U}{\partial z}\right) \tag{32}$$

$$\frac{\partial V}{\partial t} + fU = -\frac{1}{\rho}\frac{\partial P}{\partial y} + \frac{\partial}{\partial z}\left((\nu_T + \nu)\frac{\partial V}{\partial z}\right). \tag{33}$$

The horizontal pressure gradients may contain either a barotropic—due to tidal forcing—or a baroclinic—due to a horizontal density gradient—component. The equation for the density is given by [see equation (5)]:

$$\frac{\partial \rho}{\partial t} = \frac{\partial}{\partial z}\left((\lambda_T + \lambda_b)\frac{\partial \rho}{\partial z}\right). \tag{34}$$

When transport equations are used for k (KEPS2, KEPS1) and ε (KEPS2), the relevant equations are (12) and (14) without the horizontal diffusion and advection terms.

The following boundary conditions will be applied;

at the surface:

$$\rho(\nu_T + \nu)\left(\frac{\partial U}{\partial z}, \frac{\partial V}{\partial z}\right) = (\tau_{sx}, \tau_{sy})/\rho$$

$$(\lambda_T + \lambda_b)\frac{\partial \rho}{\partial z} = 0$$

$$k = \tau_s/(\rho\sqrt{c_\mu})$$

$$\varepsilon = (\tau_s/\rho)^{3/2}/(\kappa z_s) \tag{35}$$

at the bottom:

$$\rho(\nu_T + \nu)\left(\frac{\partial U}{\partial z}, \frac{\partial V}{\partial z}\right) = \rho C_D|\mathbf{U}|(U,V) = (\tau_{bx}, \tau_{by})/\rho$$

$$(\lambda_T + \lambda_b)\frac{\partial \rho}{\partial z} = 0$$

$$k = \tau_b/(\rho\sqrt{c_\mu})$$

$$\varepsilon = (\tau_b/\rho)^{3/2}/(\kappa z_b) \tag{36}$$

where τ_s, τ_b are the surface and bottom stress, z_s and z_b the distances from the surface and the bottom, and C_D is the bottom drag coefficient. The boundary conditions for k and ε are obtained by assuming equilibrium between production and dissipation of turbulence and a mixing length of the form $l = \kappa z_s$ and κz_b near the surface and the bottom.

The equations are solved numerically with a forward time-differencing scheme, evaluating the vertical diffusion terms implicitly. The Coriolis terms are determined alternatively at the old and the new time levels. A finite difference discretization in space with a staggered grid in the vertical is adopted where ν_T, λ_T, k, l and ε are stored between the points where the velocity components and the density are determined. The buoyancy term G is evaluated as the product of the old value of λ_T with the new value of the buoyancy

gradient. Sink terms in the k- and ε-equations are evaluated quasi-implicitly as recommended by Patankar (1980) and Baumert and Radach (1992). Since the currents are evaluated one half grid distance above the bottom, the bottom drag coefficient is given by

$$C_D = (\ln(0.5\Delta z/z_0)/\kappa)^{-2} \tag{37}$$

where the roughness length z_0 is chosen corresponding to a C_{100} value (drag coefficient at a reference height of 1 m) of 0.004. To prevent ε becoming infinite the boundary conditions for ε are applied one grid distance below the surface and above the bottom. The form of the boundary conditions for k and ε, which assume that the free surface acts as a solid boundary, is a commonly made assumption (e.g. Blumberg and Mellor, 1987). Alternative surface conditions which remove this constraint have been proposed by Rodi (1984). Numerical experiments with a wind-driven mixed layer (not shown) have been performed showing that the modified conditions have no significant effect on the model results.

3. EVOLUTION OF A WIND-DRIVEN SURFACE LAYER

The entrainment of a turbulent boundary layer, driven by a constant surface stress, into a stably stratified fluid is a well-known problem which has been studied both experimentally and theoretically. In the absence of the Coriolis force the problem has the interesting property that self-similar solutions exist for the equation of motion and density when the initial density profile is given by a power law or a step function in z (Kundu, 1981; Mellor and Strub, 1980; Kranenburg, 1983). This implies that the current U and the density ρ can be written in the form

$$U(z,t) = \hat{U}(t)F(\eta) \tag{38}$$

$$\rho(z,t) = \rho_h - \Delta\rho G(\eta) \tag{39}$$

where $\eta = z/h(t)$, $h(t)$ is the depth of the turbulent layer, ρ_h the density at the base of the layer, $\Delta\rho = \hat{\rho} - \rho_h$ and $\hat{U}$, $\hat{\rho}$ the mean values of current and density over the turbulent layer. When the initial stratification is linear, it can be shown that

$$h(t) = (2\overline{Ri})^{1/4} u_* (t/N_0)^{1/2}. \tag{40}$$

The solution now only depends on the two initial parameters u_* (surface friction velocity) and N_0 (initial buoyancy gradient) and the overall Richardson number $\overline{Ri}$, defined by

$$\overline{Ri} = N_0^2 h^2/(2\hat{U}^2). \tag{41}$$

The parameter $\overline{Ri}$ is constant in space and time if one assumes that the Richardson number is equal to a critical value Ri_c at the bottom of the turbulent layer. The theory of sections 2.4 and 2.5 shows that this will be true for the three turbulence schemes provided that production and dissipation of turbulence are in balance at $z = -h(t)$. From the self-similarity theory it follows then that $\overline{Ri}$ depends only on the choice of the turbulence scheme. The validity of the self-similarity hypothesis depends also on the implicit

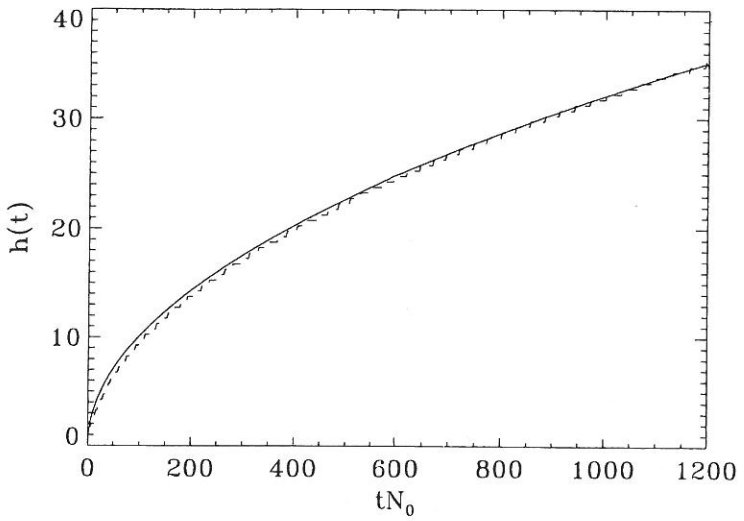

Fig. 3. Evolution of the turbulent layer depth (m) vs the dimensionless time tN_0 according to the self-similarity relation (40) with $\overline{Ri} = 0.53$ and the KEPS2 model.

assumption that the turbulent fluxes of momentum and density can also be cast into a self-similar form. As shown by Kundu (1981) this requires that

$$\nu_T, \lambda_T \sim \frac{h^2}{t} f(\eta). \tag{42}$$

Although this appears to be true for a two-layer stratification, this is not the case for the linearly stratified problem. To test the self-similarity hypothesis the KEPS2 model is run with $N_0 = 10^{-2}\,\mathrm{s}^{-1}$ and $u_* = 10^{-2}\,\mathrm{m\,s}^{-1}$. Time step and vertical grid spacing are given by $\Delta z = 0.5\,\mathrm{m}$ and $\Delta t = 50\,\mathrm{s}$. To remove the effects of the bottom boundary layer a sufficiently large water depth of $H = 100\,\mathrm{m}$ is chosen. The turbulent layer depth is defined as the point where the condition $|\rho(z) - \rho_{\mathrm{in}}(z)| \leq 0.01|\rho(z) - \rho_s|$ is first satisfied where $\rho_{\mathrm{in}}(z)$ is the initial density profile and ρ_s the surface density. The simulation yields an almost constant value of $\overline{Ri}$ when $tN_0 \gtrsim 200$–300. Figure 3 shows the evolution of $h(t)$. The results compare well with the theoretical curve using the value $\overline{Ri} = 0.53$ obtained from the calculations. Similar results apply for the two other models. Profiles of the dimensionless velocity $F(\eta)$ and density $G(\eta)$ at different times are illustrated in Fig. 4(a) and (b). One observes a mixed layer which extends to a depth of $z \simeq -0.4\,\mathrm{h}$. A transition layer is situated beneath this layer where the density continuously increases towards its undisturbed initial value. A similar density structure has been measured by Kranenburg (1984) for the case of a two-layer stratification. It is clear that after removal of the initial conditions ($tN_0 \gtrsim 100$) self-similarity prevails (at least for $tN_0 \lesssim 1200$) throughout the turbulent layer with exception of the surface layer where a reduction in surface velocity can be observed. This appears to contradict the earlier results of Kundu (1981). In his simulations the self-similarity breaks down when a sharp pycnocline forms at the bottom of the turbulent layer. This occurs when $tN_0 \gtrsim 500$ which is much earlier than the simulation

period of $tN_0 = 1200$ used in the present case. As a final test Fig. 4(c) shows a time series of eddy viscosity profiles using the dimensionless form (42). It can be seen that self-similarity is well approximated in the transition layer ($z < -0.4$ h). Within the surface layer viscosity increases stronger in time than expected from the self-similarity form (42). This explains the reduction in surface shear and velocity, observed in Fig. 4(a).

Laboratory experiments on mixed layer deepening under the action of a surface stress were conducted by Kato and Phillips (1969) who used an annular tank which contained initially a fluid with a constant density gradient. Contrary to the self-similar solution (40), they found that the turbulent layer increases in time like $t^{1/3}$. Price (1979a) showed that the Kato–Phillips data are influenced by the presence of the side-walls. This effect was eliminated by the inclusion of a side-wall friction term in the equation of motion. A similar analysis was performed by Thompson (1979). It then appeared that the data are in good agreement with a relation of the form (40), giving support to the self-similarity hypothesis. It is now clear that a comparison between numerical and experimental or observational results should concentrate in the first place on the evaluation of the critical parameter $\overline{Ri}$. A series of values obtained from experimental and observational data and previous model simulations is listed in Table 1. Most of them are situated within the range $\overline{Ri} \simeq 0.6$–0.8. Exceptions are the value $\overline{Ri} = 1$, which was assumed a priori by Pollard *et al.* (1973) and $\overline{Ri} = 0.35$ obtained by Mellor and Durbin (1975) with a local equilibrium scheme similar to the KEPS0 model.

Values of $\overline{Ri}$ for the three models using different initial conditions and two vertical resolutions $\Delta z = 0.5$ m and $\Delta z = 2$ m are given in Table 2. Vertical profiles of the dimensionless velocity and density at the end of the simulation ($tN_0 = 1200$) are illustrated in Fig. 5(a) and (b). The algebraic length scale in the KEPS1 and KEPS0 models is prescribed by the Blackadar formula (20) and (21) with $\gamma = 0.2$ and stratification accounted for by the limiting condition (29) for l. The results of the KEPS2 and KEPS1 model are very similar yielding a value somewhat below the one obtained by Price (1979a) and below the range derived by Thompson (1979) from the Kato–Phillips data. The bulk Richardson number is practically independent of the initial conditions and the vertical grid resolution. The results with the KEPS0 model are less satisfactory. In the case where $\Delta z = 2$ m the overall Richardson number varies more strongly with the initial conditions. When the vertical resolution is reduced to $\Delta z = 0.5$ m, it can be seen that $\overline{Ri}$ strongly depends on the initial conditions and has a much lower value. A comparison with Mellor and Durbin (1975)'s value $\overline{Ri} = 0.35$ seems to indicate that the latter result must be related to the local equilibrium assumption in the turbulent energy equation. The model also produces a 'jiggling' pattern both in density and in current, situated in the middle of the layer. This behaviour is related to strong oscillations in space and time of the profiles of eddy viscosity and diffusivity (not shown). A similar problem has been reported by Frey (1991) who used the Mellor–Yamada level 2 equilibrium closure scheme. He showed that this instability disappears when Δz is taken sufficiently large or Δt sufficiently small. Taking account of those limitations it can be verified that the KEPS0 model is more closely in agreement with the other two models.

4. TIDALLY INDUCED PERIODIC STRATIFICATION

In the previous section a rather idealized problem was considered (no Coriolis force, constant wind stress), enabling comparison of the different turbulent closures in a simple way using only the constant surface stress and initial density gradient as input parameters.

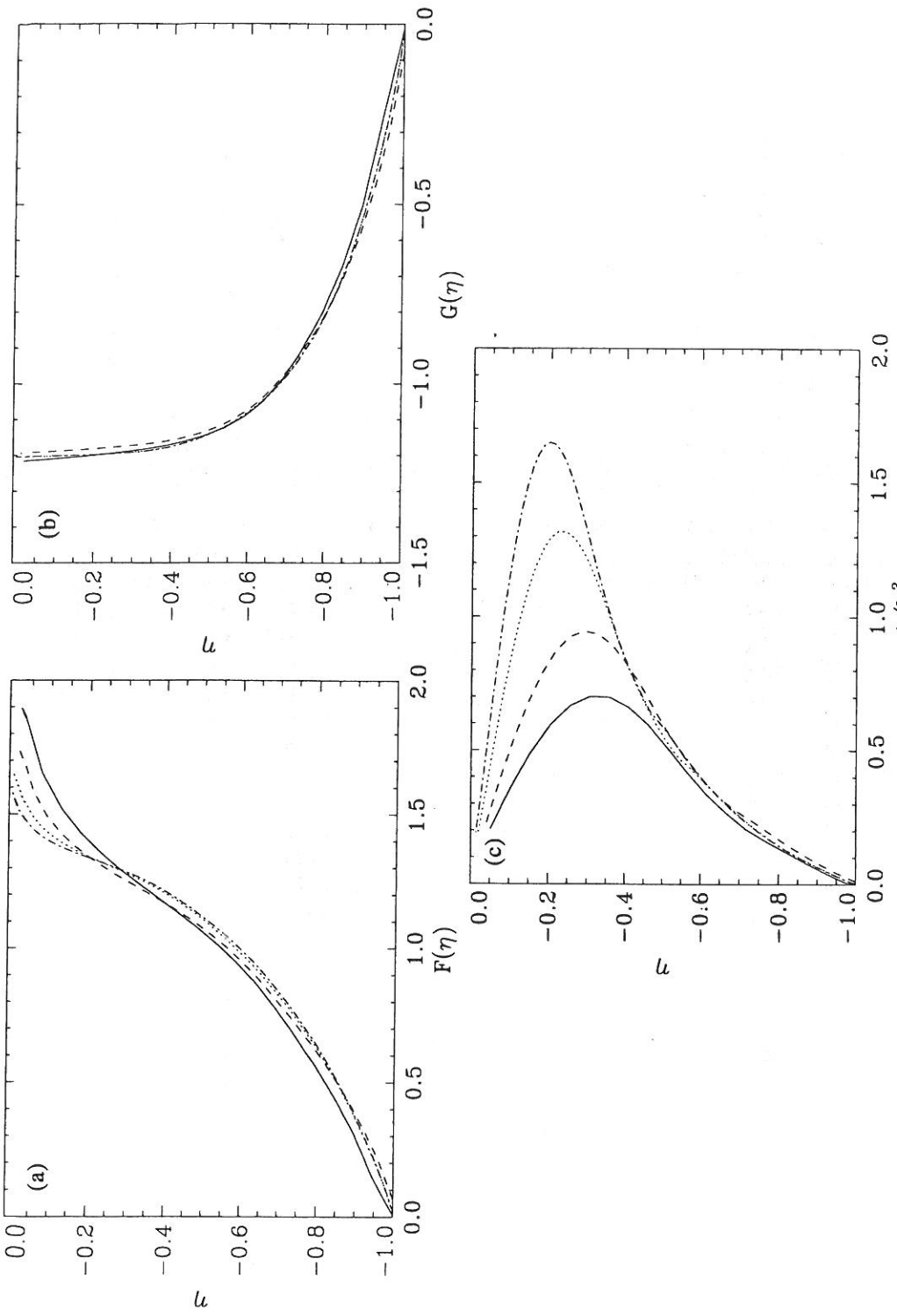

Fig. 4. (a) Dimensionless velocity profiles $F(\eta)$ using the KEPS2 model and $\Delta z = 0.5$ m, $\Delta t = 50$ s at $tN_0 = 100$ (solid), 200 (dashes), 600 (dots), 1200 (dash-dots). (b) As (a), now for the dimensionless density $G(\eta)$. (c) As (a), now for the dimensionless eddy viscosity $\nu_T t/h^2$.

Table 1. Values of the global Richardson number $\overline{\mathrm{Ri}}$ *according to different authors*

Source	Method	$\overline{Ri}$
Pollard *et al.* (1973)	Analytical	1.0
Mellor and Durbin (1975)	Equilibrium $k - l$ turbulence model	0.35
Price (1979a)	Data of Kato–Phillips experiments	~0.6
Price (1979b)	Oceanographic measurements	~0.6
Thompson (1979)	Data of Kato–Phillips experiments	0.7–1.0
Kundu (1981)	Gibson–Launder $k - \varepsilon$ turbulence model	0.6
Trowbridge (1992)	Analytical	0.74

In this section a more realistic case of shelf sea stratification will be studied where the horizontal pressure and density gradient and the Coriolis force will be included. The turbulence models will be applied to simulate the periodic variation of stratification in a region where freshwater (buoyancy) is supplied by the river Rhine. This ecologically important ROFI extends northeastwards along the Dutch coast from the mouth of the river Rhine and typically up to a distance of ~30 km from the coast (Fig. 6). The time evolution of stratification and currents was studied by shipboard CTD, fixed moorings and H/F radar in September and October 1990 (Simpson *et al.*, 1993; Bos *et al.*, 1992). A time series of the bottom-surface density difference [Fig. 10(c)] shows that the water column was almost completely mixed during the period of springs (6–10 October) which coincides with a period of strong winds [Fig. 10(a)]. Stratification redevelops during neaps (12–16 October) which is a period of low winds. This semi-monthly variability is modulated by semi-diurnal oscillations which are small at springs but increase in amplitude during neaps.

The basic approximation necessary to represent the physics with the aid of a one-dimensional model is that the horizontal advection of freshwater and the baroclinic pressure gradient are modelled using the assumption of an across shore horizontal density

Table 2. Dependence of the global Richardson number $\overline{\mathrm{Ri}}$ *on wind stress and stratification for different resolutions*

$N_0^2(\mathrm{s}^{-2}) \times 10^4$	$u_*(\mathrm{m\,s}^{-1}) \times 10^2$	KEPS2	KEPS1	KEPS0
			$\Delta z = 0.5$ m	
1.0	1.0	0.53	0.51	0.45
1.0	2.0	0.53	0.51	0.13
10.0	2.0	0.54	0.53	0.41
10.0	4.0	0.55	0.54	0.10
			$\Delta z = 2$ m	
1.0	1.0	0.49	0.47	0.54
1.0	2.0	0.52	0.49	0.62
10.0	2.0	0.49	0.49	0.64
10.0	4.0	0.53	0.52	0.75

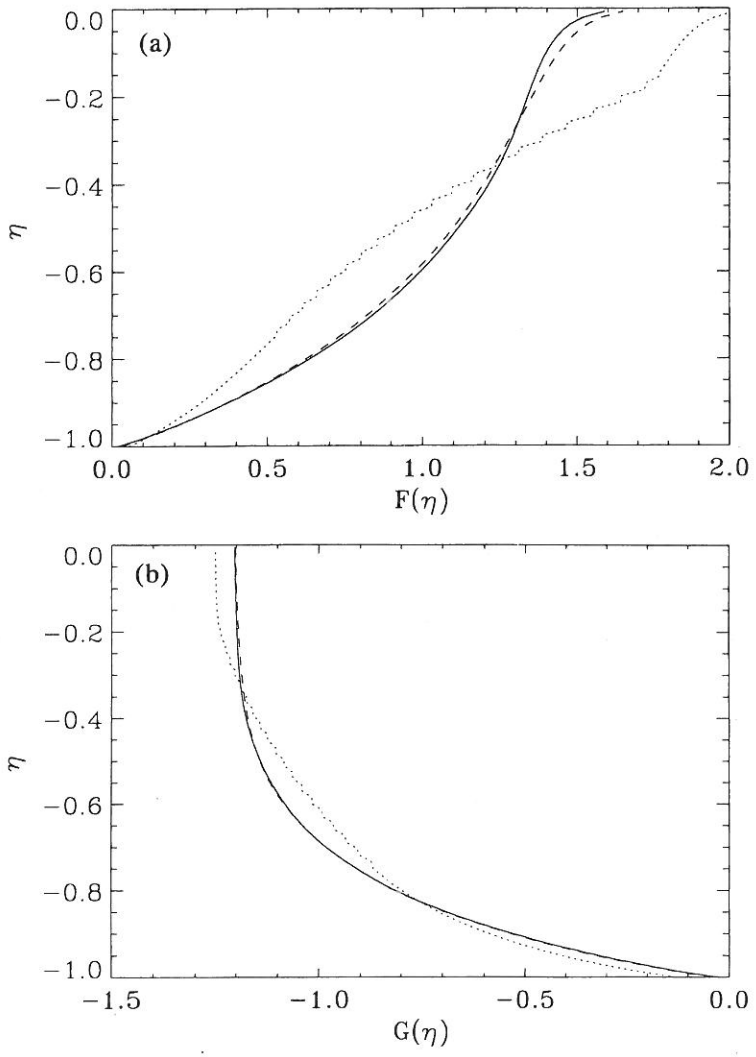

Fig. 5. (a) Dimensionless velocity profile $F(\eta)$ at $tN_0 = 1200$ using $\Delta z = 0.5$ m, $\Delta t = 50$ s and the KEPS2 (solid), KEPS1 (dashes), KEPS0 (dots) model. (b) As (a), now for the dimensionless density $G(\eta)$.

gradient, constant over depth and time. The momentum and density equations are then similar to those applied successfully by Simpson and Sharples (1992) to describe the springs–neaps cycle in Liverpool Bay. Horizontal advection and diffusion of momentum and the turbulent quantities k and ε are neglected so that (32) and (33) apply here where the x-axis is now oriented southeastwards antiparallel to the horizontal density gradient and the y-axis northeastwards parallel to the coast (Fig. 6). The vertical coordinate z increases from $-H$ at the bottom to η at the surface, where η is the surface elevation. The across shore pressure gradient is evaluated by integrating the equation of vertical

hydrostatic equilibrium and using the assumption that $\partial\rho/\partial x$ is independent of depth (see Officer, 1976). This gives

$$-\frac{1}{\rho}\frac{\partial P}{\partial x} = -\frac{1}{\rho}\frac{\partial}{\partial x}\int_z^\eta \rho g \, dz$$

$$= -g\frac{\partial \eta}{\partial x} - \frac{g}{\rho}\int_z^\eta \frac{\partial \rho}{\partial x} dz$$

$$\simeq -g\frac{\partial \eta}{\partial x} - \frac{g}{\rho}\int_z^0 \frac{\partial \rho}{\partial x} dz$$

$$\simeq -g\frac{\partial \eta}{\partial x} + \frac{1}{\rho}\frac{\partial \rho}{\partial x} gz. \tag{43}$$

Density gradients in the along shore direction are typically much smaller than in the across shore direction and are neglected here. The momentum equations then take the form

$$\frac{\partial U}{\partial t} - fV = -g\frac{\partial \eta}{\partial x} + \frac{1}{\rho}\frac{\partial \rho}{\partial x} gz + \frac{\partial}{\partial z}\left((\nu_T + \nu)\frac{\partial U}{\partial z}\right) \tag{44}$$

$$\frac{\partial V}{\partial t} + fU = -g\frac{\partial \eta}{\partial y} + \frac{\partial}{\partial z}\left((\nu_T + \nu)\frac{\partial V}{\partial z}\right). \tag{45}$$

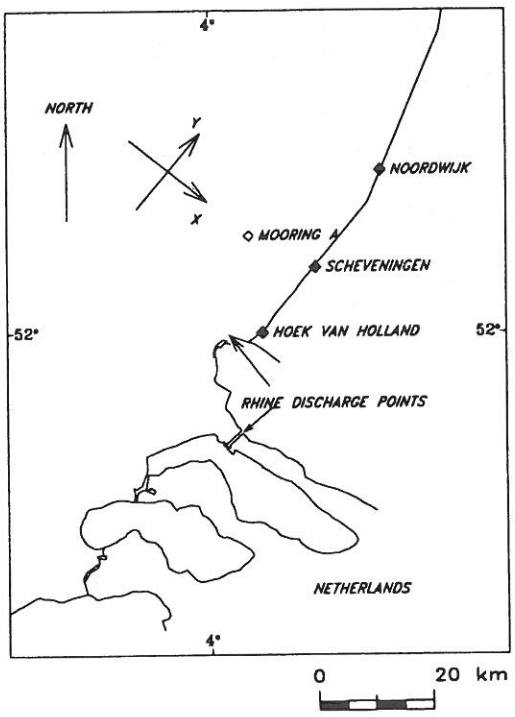

Fig. 6. Map of the Dutch coastal zone with location of the mooring and direction of the coordinate axes.

The equation of density now contains a term representing horizontal advection of density:

$$\frac{\partial \rho}{\partial t} = -U\frac{\partial \rho}{\partial x} + \frac{\partial}{\partial z}\left((\lambda_T + \lambda_b)\left(\frac{\partial \rho}{\partial z}\right)\right). \tag{46}$$

Equations (44)–(46) describe the vertical and temporal structure of current and density, considering the horizontal derivatives ($\partial\eta/\partial x$, $\partial\eta/\partial y$, $\partial\rho/\partial x$) as applied forcing terms. The across shore surface pressure gradient $\partial\eta/\partial x$ is found by supposing that the sea surface adjusts to ensure that the vertically integrated across shore current is always zero. This crucial assumption is justified theoretically by Visser *et al.* (1994), who argue that when close (i.e. much smaller than the barotropic Rossby radius) to the coast, where $\overline{U} = 0$ exactly, this is a good approximation, and is supported by current measurements, which show oppositely directed bottom and surface across shore currents. The across shore surface slope can now be eliminated by substracting equation (44) and its depth averaged counterpart, using the assumption $\overline{U} = 0$, to obtain,

$$\frac{\partial U}{\partial t} - f(V - \overline{V}) = \frac{1}{\rho}\frac{\partial \rho}{\partial x} g\left(z + \frac{H}{2}\right) + \frac{\partial}{\partial z}\left((\nu_T + \nu)\frac{\partial U}{\partial z}\right) - \frac{\tau_{sx} - \tau_{bx}}{H} \tag{47}$$

where a bar denotes a depth averaged value. The along shore pressure gradient is modelled by assuming that the tidal elevation can be approximated as a progressive (Kelvin) wave propagating up the Dutch coast. Thus,

$$\eta = \sum_{i=1}^{N} \eta_{0i}(x) \cos\left(\omega_i\left(t - \frac{y}{c}\right) - \phi_{0i}\right) \tag{48}$$

where i ranges over N tidal constituents with angular speed ω_i, amplitude η_{0i} and phase ϕ_{0i}, and $c = \sqrt{gH}$ is the tidal propagation speed. Thus,

$$-g\frac{\partial \eta}{\partial y} = \sum_{i=1}^{N} A_i \cos(\omega_i t - \phi_i). \tag{49}$$

The two dominant tidal components (M_2 and S_2) will be considered in the subsequent analysis. Using $\eta_{01} = 0.62$ m, $\eta_{02} = 0.15$ m and $H = 20$ m one obtains

$$(A_1, A_2) = (0.61, 0.16) \times 10^{-4}\ \mathrm{m\,s^{-2}} \tag{50}$$

while optimum agreement with the data is obtained by choosing $\phi_1 = 45°$, $\phi_2 = 15°$.

A first series of simulations has been made with only one (M_2) tidal component and without wind stress. In this way insight can be gained into the physical processes, leading to stratification or destratification, and a clear comparison can be made between the different schemes. The models are run using $\Delta t = 180$ s, $\Delta z = 1$ m. The across shore density gradient is estimated from CTD transects (Bos *et al.*, 1992) as $\rho^{-1}\partial\rho/\partial x = -2.3 \times 10^{-7}\ \mathrm{m^{-1}}$. Time series of the bottom-surface density difference according to the KEPS2 and KEPS1 models are shown in Fig. 7. In the latter case a mixing length is used of the form (22) with l limited according to (29). Both models predict a semi-diurnal variation in stratification on which a small inertial oscillation is superimposed. Due to the interaction between the two types of oscillation the amplitude of the semi-diurnal oscillation varies with the period $T = 2\pi/(\omega_1 - f) = 5.4$ times the tidal period where ω_1 is the frequency of the M_2-tide. It

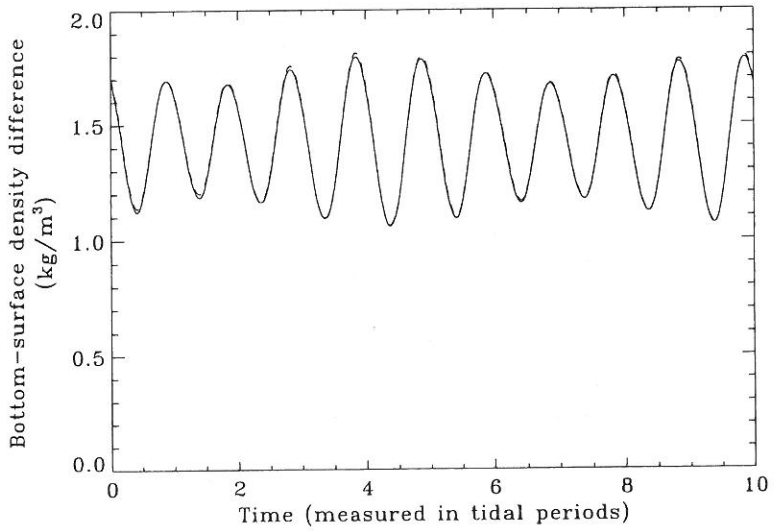

Fig. 7. Bottom-surface density difference in kg m^{-3} according to the KEPS2 (solid) and KEPS1 (dashes) model with one tidal forcing component and without wind stress.

can be seen that the results are practically the same. In view of this small difference only the simpler KEPS1 model will be considered in the subsequent analysis.

The time evolutions of different quantities during two tidal periods are displayed in Fig. 8(a)–(f). Contour plots of the across shore and along shore currents, the density and the eddy viscosity are shown in Fig. 8(a)–(d). Time series of the bottom-surface density difference and the depth averaged along shore velocity are shown in Fig. 8(e)–(f). The presence of a residual stratification [Fig. 8(e)] can be deduced by solving the time-independent momentum equations (44) and (45) for a constant eddy viscosity. Details can be found in Heaps (1972). It then appears that an offshore flow is produced near the surface and an onshore flow near the bottom. This across shore circulation advects fresh (salt) water near the surface (bottom) producing a stratified water column. As described by Visser *et al.* (1994) the tidal currents which are predominantly along shore, rotate anticyclonically with depth. This can be seen by comparison of Figs 8(a) and (b). The across shore and along shore velocities are ~90° out of phase in agreement with the current observations in the near-shore region (Bos *et al.*, 1992). The tidal across shore circulation advects freshwater, increasing stratification over the half tidal cycle of offshore surface current and reducing stratification during onshore surface current. Extrema of stratification, as represented by the bottom-surface density difference [Fig. 8(e)], occur at moments of across shore current reversal. A detailed description of the effect of tidal straining can be found in Simpson *et al.* (1990) for Liverpool Bay. The evolution of turbulence during a tidal cycle can be deduced from Fig. 8(d). A bottom boundary layer due to the tidal shear of the along shore current is clearly visible. Within this layer turbulence varies with a quarterly diurnal period. Comparison with Fig. 8(b) shows that viscosity is maximal when $|V_z|$ has its largest value. A second turbulence maximum is situated near the middle of the fluid column ($z \simeq -12$ m). Contrary to the bottom layer turbulence evolves here on a semi-diurnal time scale in response to advection-induced semi-diurnal variation of stratification.

A second test has been performed where the KEPS1 model is run still without wind stress but with two components (M_2 and S_2) in the tidal forcing. The time evolution over a springs–neaps cycle of the depth averaged along shore velocity and the bottom-surface density difference, together with their values averaged over a M_2-tidal cycle, are shown in Fig. 9(a) and (b). It can be seen that stratification is reduced at springs, while it increases during neaps. The semi-diurnal oscillations are larger at springs than during neaps. The evolution can be explained physically by analysing the time-evolution equation for the potential energy anomaly, defined by

$$\Phi = \frac{1}{H}\int_{-H}^{0} (\bar{\rho} - \rho) g z \, dz \tag{51}$$

which represents the amount of energy, required to bring about complete mixing (Simpson *et al.*, 1990). Integrating the density equation (46) over the vertical one obtains

$$\frac{\partial \Phi}{\partial t} = \frac{g}{H}\frac{\partial \rho}{\partial x}\int_{-H}^{0} Uz \, dz + \frac{g}{H}\int_{-H}^{0} \lambda_T \frac{\partial \rho}{\partial z} \, dz. \tag{52}$$

The first term on the right describes the influence on stratification of the advection by the across shore current. The second one represents the (tidal) mixing rate. The time evolution of the two quantities are illustrated in Fig. 9(c) and (d). Comparison of Figs 8(b) and (d) shows that turbulence is generated mainly by the along shore current. At neaps turbulent mixing is therefore minimal. This is not compensated by an analogous increase in stratification, which explains the reduction of the tidal mixing rate at neaps visible in Fig. 9(d). This figure shows also that the tidally averaged across shore current decreases during neaps, which can be explained in the following way. Heaps (1972)'s analytical study shows that the viscous term in the across shore momentum equation increases with respect to the Coriolis acceleration during springs, producing an increased shear flow in the across shore direction. At neaps, when viscosity is reduced, the Coriolis term becomes more dominant except near the sea bed where bottom friction is still important. This tendency towards a geostrophic balance increases the along shore current with respect to the across shore component. Figure 9(d) shows that the increase of averaged stratification at neaps is due to the fact that tidal mixing decreases more rapidly than the advective term just before neaps. The opposite is true just before springs. Tidal mixing now grows more strongly than the advective term so that stratification is reduced at springs.

Finally, simulations have been made with the KEPS1 model using meteorological forcing data and with two tidal components. The simulated period ranges from 1 to 20 October 1990 which covers an entire springs–neaps cycle. Figure 10(a)–(c) show time series of respectively the magnitude and direction of the surface stress and the bottom-surface density difference, which are taken from Simpson *et al.* (1993). The wind stress is calculated using the drag relation (Geernaert *et al.*, 1986)

$$\boldsymbol{\tau}_s = \rho_a 10^{-3}(0.43 + 0.097|\boldsymbol{U}_{10}|)|\boldsymbol{U}_{10}|\boldsymbol{U}_{10} \tag{53}$$

where $\boldsymbol{U}_{10}$ is the wind velocity at 10 m above the surface, measured at Hook of Holland, and ρ_a the density of air. The density difference, measured between 1 and 16 m below the surface, has been obtained at a mooring, situated at 52.2° N, 4.1° E and at a distance of 7 km from the coast (Fig. 6).

The density difference and the depth averaged along shore velocity according to the

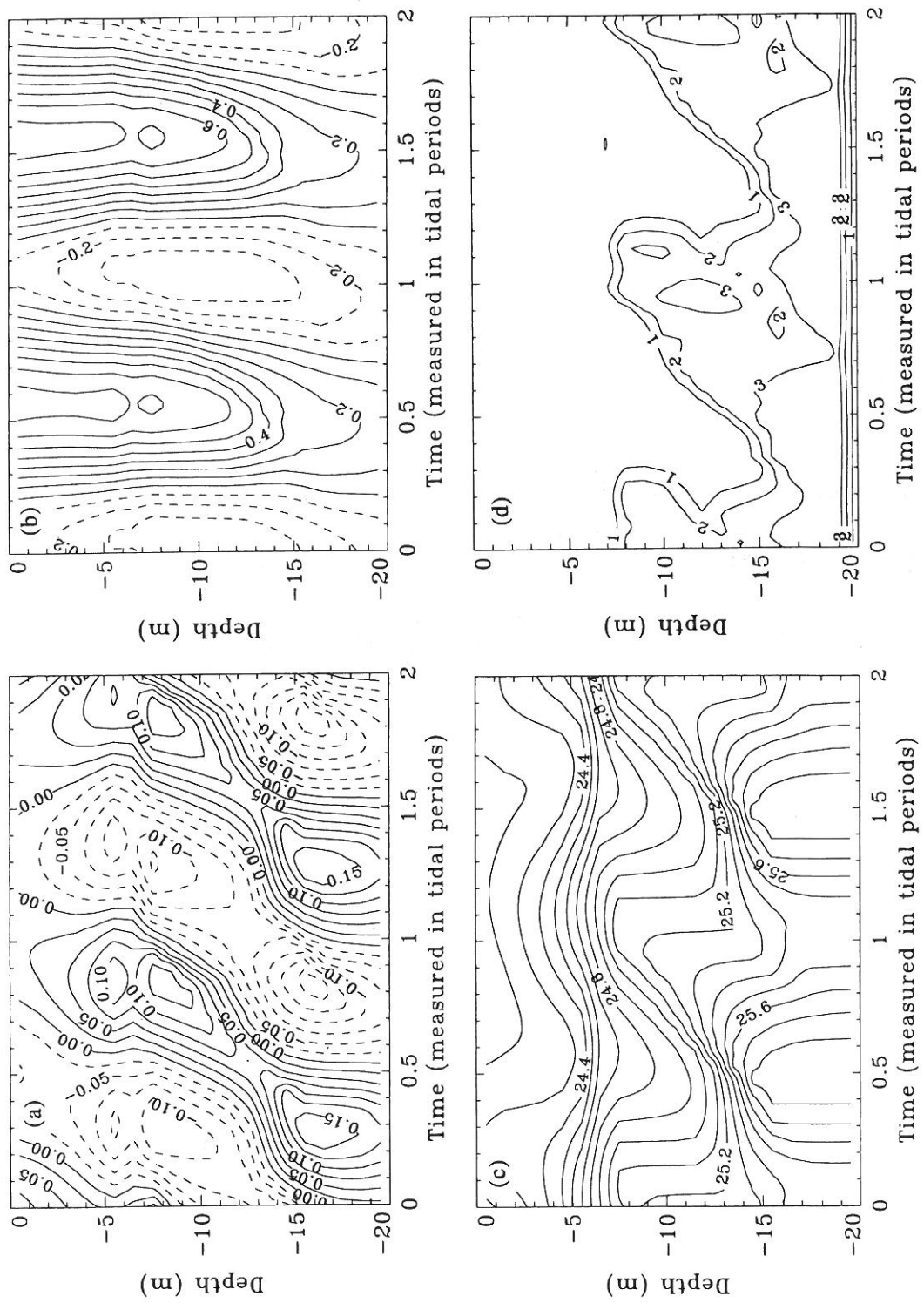
(a)
(b)
(c)
(d)
Depth (m)
Time (measured in tidal periods)
0
-5
-10
-15
-20
0.5
1
1.5
2

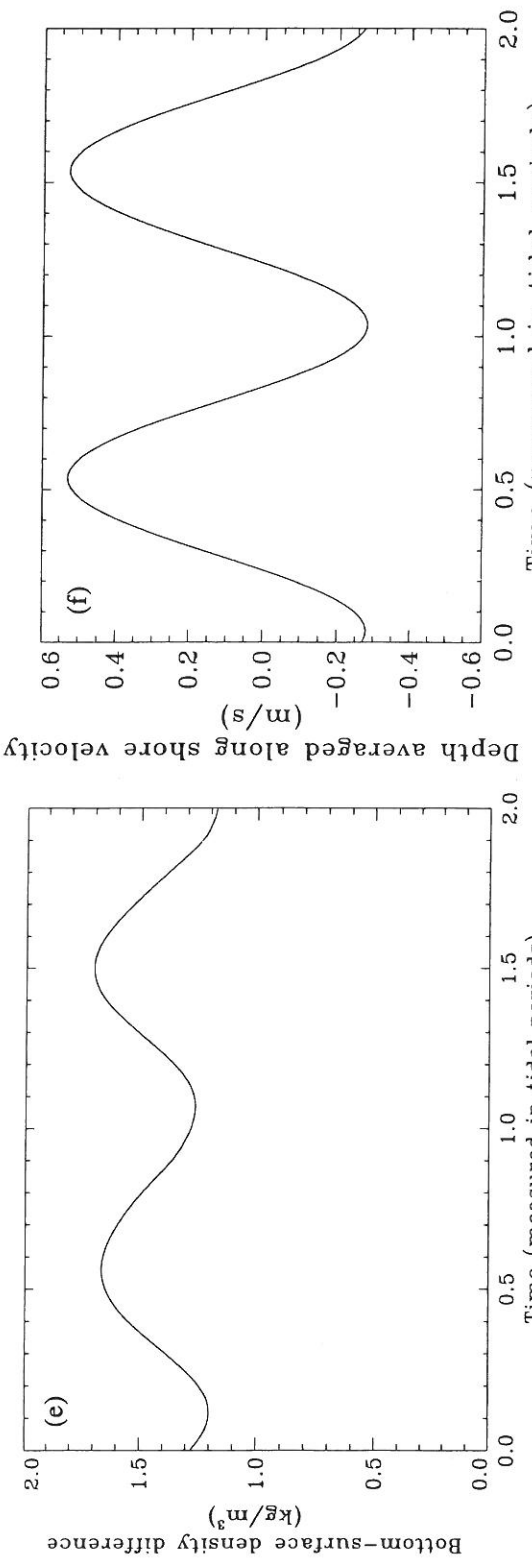

Fig. 8. (a) Contour plot of the across shore current ($m\,s^{-1}$) over two tidal cycles (solid: onshore, dashes: offshore) with one tidal forcing component. (b) As (a), now for the along shore current ($m\,s^{-1}$) (solid: northeastwards, dashes: southwestwards). (c) As (a), now for the density $\rho - 1000\ kg\ m^{-3}$. (d) As (a), now for $\log(10^6 \nu_T)$ with ν_T in $m^2\,s^{-1}$. (e) Time series of the bottom-surface density difference ($kg\ m^{-3}$) over two tidal cycles with one tidal forcing component. (f) As (e), now for the depth averaged along shore current ($m\,s^{-1}$).

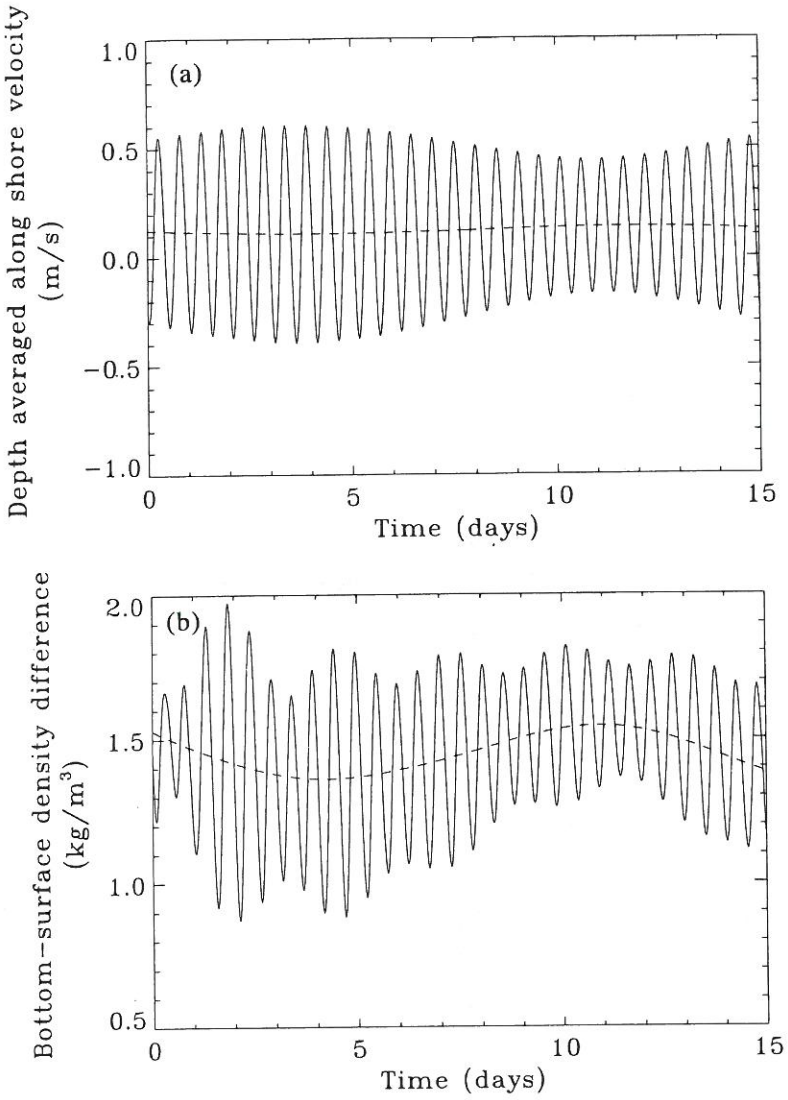

Fig. 9. (a) Time series of the depth averaged along shore current in m s^{-1} (solid) and its average over a M_2-tidal cycle (dashes) with two tidal forcing components. (b) As (a), now for the bottom-surface density difference (kg m^{-3}). (c) Time series of the advective term (kg m^{-1} s^{-3}) in the potential energy anomaly equation (52). (d) Time series of the tidal mixing rate (kg m^{-1} s^{-3}), its tidal average (dashes) and the tidally averaged advection term (dots).

model simulations are illustrated in Fig. 10(d) and (e), respectively. It can be observed that the model reproduces at least some aspects of the data. Stratification is weak during springs (6–10 October) while strong during neaps (12–16 October). The isolated peaks at 5 and 8–9 October, which are associated with a sharp decrease in wind stress, are well predicted by the model. Wind effects influence the results in two ways. Advection by wind-induced currents can enhance or reduce stratification depending on the wind direction.

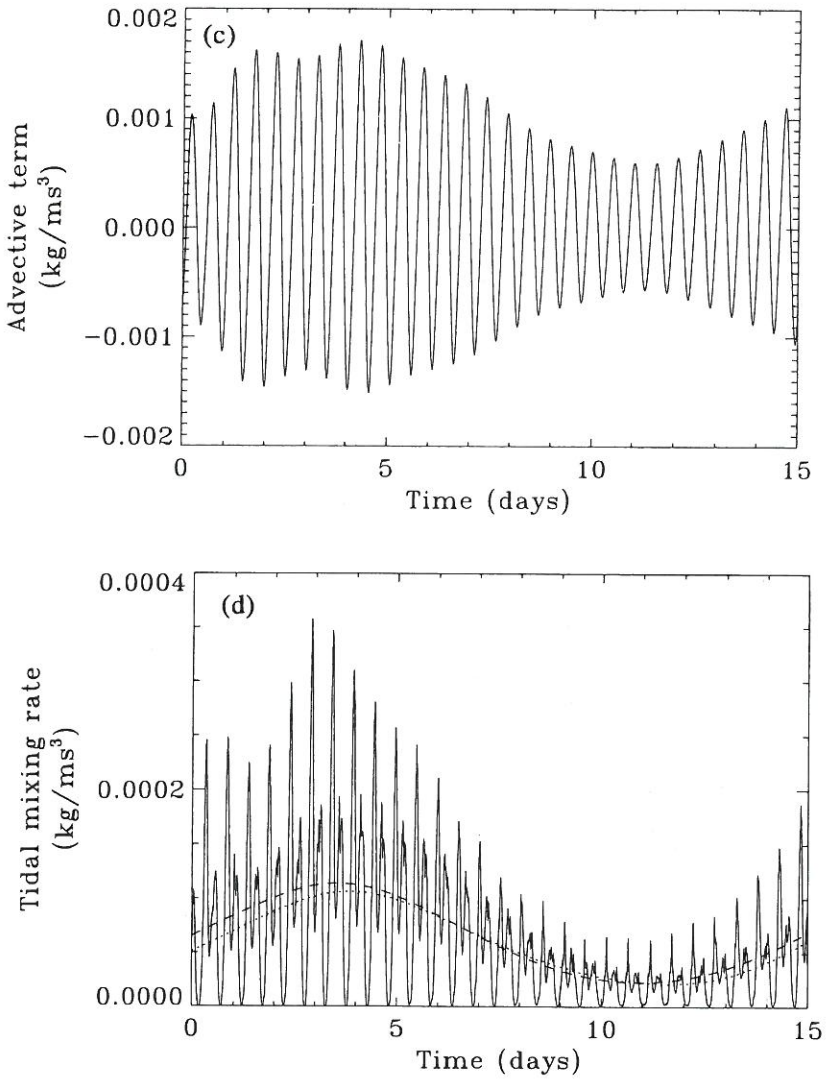

Fig. 9. *Continued.*

Additional simulations (not shown) indicate that stratification increases for low onshore winds, which may explain the maximum at 8–9 October. The opposite is true for offshore winds. On the other hand, wind mixing will reduce the vertical density gradient in the surface layer.

Fig. 10 (*on following pages*). (a) Magnitude of wind stress (N m^{-2}) during the period of 1–20 October 1990 using meteorological data at Hook of Holland. (b) Direction of the wind stress (degrees) during the period of 1–20 October 1990 (0°: onshore, 180°: offshore). (c) Observed values of the density difference (kg m^{-3}) between 1 and 16 m below the surface at 52.2° N, 4.1° E during the period of 1–20 October 1990. (d) Time series of the bottom-surface density difference (kg m^{-3}) according to the KEPS1 model and using meteorological forcing data. (e) As (d), now for the depth averaged along shore velocity (m s^{-1}). (f) As (d), now for the advective term (kg m^{-1} s^{-3}) in the potential energy anomaly equation (52). (g) As (d), now for the tidal and wind mixing rate (kg m^{-1} s^{-3}).

(a)
(b)
(c)
(d)
Magnitude of wind stress
(N/m²)
Direction of surface stress
(degrees)
Bottom–surface density difference
in kg/m³ (data)
Bottom–surface density difference
in kg/m³ (model)
October

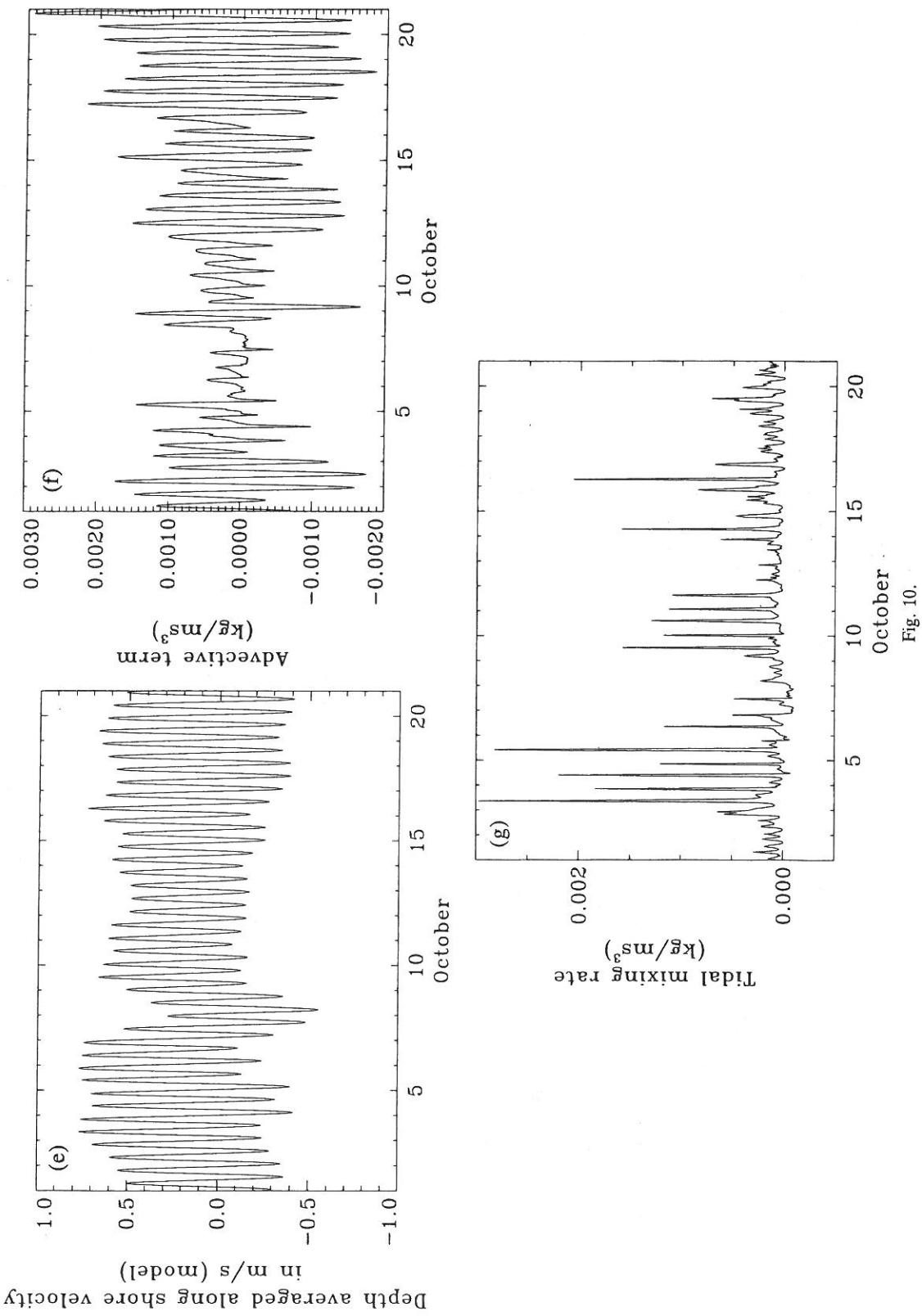
Depth averaged along shore velocity
in m/s (model)
(e)
1.0
0.5
0.0
−0.5
−1.0
5
10
15
20
October
Advective term
(kg/ms³)
(f)
0.0030
0.0020
0.0010
0.0000
−0.0010
−0.0020
5
10
15
20
October
Tidal mixing rate
(kg/ms³)
(g)
0.002
0.000
5
10
15
20
October

Fig. 10.

The sharp maxima, visible in the data at 2 October and during 12–15 October, appear to be underestimated by the model by a factor ~2. A clear explanation is lacking. Improvements could in principle be made by increasing the horizontal density gradient. Additional simulations showed that while this increases the stratification during neaps, the large semi-diurnal oscillations are not produced. It should be noted however that other data sets, obtained at a different mooring station during the same period, show a less significant increase in stratification (Bos *et al.*, 1992). The results are clearly not in agreement with those obtained in the absence of wind forcing [Fig. 9(b)]. To illustrate this, the time evolution of the two terms on the right of (52) (advective term and mixing rate) with wind forcing are shown in Fig. 10(f) and (g). It can be seen that the across shore currents and their semi-diurnal oscillations are now larger at neaps than during springs in agreement with the observations (Visser *et al.*, 1994). Comparison of Figs 9(d) and 10(g) shows that turbulent mixing is mostly produced by the wind. Probably the main cause of discrepancies between model and observations is the representation of the horizontal density gradient, which is taken as depth and time independent. Forcing the model with time-varying measured density gradients may improve the results (A. J. Souza, private communication). Along shore advection of freshwater, not represented by the model, may also contribute to the observed stratification signal (A. Visser, private communication).

5. SUMMARY AND CONCLUSIONS

Three turbulence closure schemes, designed for stratified flows in shallow waters, have been presented and tested. They may be considered as three versions of the same model with the exception that each one uses a different number of transport equations for turbulence variables. The models are first tested on the evolution of a wind-driven turbulent layer without Coriolis force. The rate of entrainment predicted by the KEPS2 and KEPS1 models agrees well with the observational data and the results of laboratory experiments. The evolution of the turbulent layer depth, density and current profiles are in good agreement with the self-similarity hypothesis. Contrary to the earlier investigation by Kundu (1981) the development of a sharp interface at larger times is not confirmed by the present study. In analogy with Frey (1991) the KEPS0 model is susceptible to numerical instabilities arising when Δt is too high or Δz too small.

The model results are at least qualitatively in agreement with data when applied to simulate the stratification in the Rhine plume, despite model simplifications—neglection of along shore advection, simplified tidal forcing parameters and constant horizontal density gradient. The springs–neaps cycle of stratification is fairly predicted by the simulations. The large semi-diurnal oscillations which according to the data reach amplitudes of the order of 4–6 kg m^{-3} at neaps, are also visible in the model runs but with a lower amplitude. In analogy with the theory explained in Simpson *et al.* (1990) and Heaps (1972) the processes which induce or destroy stratification are advection by the wind-induced and tidal residual currents, tidal straining and turbulent mixing.

The results of the KEPS2 and KEPS1 models are very similar. This indicates that there is no need, at least for the type of problems discussed in this paper, for solving an additional equation for the turbulent dissipation. At the next stage, the turbulence models will be incorporated into an existing three-dimensional baroclinic circulation model (Ruddick *et al.*, 1994). This may allow for a better quantitative comparison with the observations and will be the subject of forthcoming investigations.

Acknowledgements—This research was funded by the European Community under contract MAST-0050-C-PROFILE. The second and third authors are working in the scope of contract GC/10/013, respectively GC/58/015 (Belgian State, Prime Minister's Services, Science Policy Office). The fourth author was funded by the European Community under contract MAST-900064. J. Simpson and A. Souza (School of Ocean Studies, UCNW) are thanked for providing the data of the October 1990 Rhine plume campaign. Colleagues in the PROFILE group and in particular A. Visser (University of Utrecht) are acknowledged for advice and critical comments on modelling the Rhine outflow area.

REFERENCES

Baum E. and E. A. Caponi (1992) Modeling the effects of buoyancy on the evolution of geophysical boundary layers. *Journal of Geophysical Research*, **97**, 15,513–15,527.

Baumert H. and G. Radach (1992) Hysteresis of turbulent kinetic energy in non-rotational tidal flows: a model study. *Journal of Geophysical Research*, **97**, 3669–3677.

Blackadar A. K. (1962) The vertical distribution of wind and turbulent exchange in a neutral atmosphere. *Journal of Geophysical Research*, **67**, 3095–3102.

Blumberg A. F. and G. L. Mellor (1987) A description of a three-dimensional coastal ocean circulation model. In: *Three-dimensional coastal ocean models, coastal and estuarine sciences 4*, N. S. Heaps, editor, American Geophysical Union, Washington, pp. 1–16.

Bos W. G., A. W. Visser, C. Heins, G. J. Kolle and P. C. Beukenkamp (1992) Rhine plume experiment—data report Holland surveys—October 1990. Report DGW-92.020, MAST-0050-C, Tidal Waters Division, Rijkswaterstaat, Netherlands.

Crawford W. R. (1986) A comparison of length scales and decay times of turbulence in stably stratified flows. *Journal of Physical Oceanography*, **16**, 1847–1854.

Davies A. M. and J. E. Jones (1990) Application of a three-dimensional turbulence energy model to the determination of tidal currents on the Northwest Continental Shelf. *Journal of Geophysical Research*, **95**, 18,143–18,162.

Deleersnijder E. (1992) A note on the stability functions of the Mellor–Yamada level 2.5 turbulence closure. *Bulletin de la Société Royale des Sciences de Liège*, **61**, 397–404.

Deleersnijder E. and P. Luyten (1994) On the practical advantages of the quasi-equilibrium version of the Mellor and Yamada level 2.5 turbulence closure applied to marine modelling. *Applied Mathematical Modelling*, **18**, 281–287.

Dickey T. D. and G. L. Mellor (1980) Decaying turbulence in neutral and stratified fluids. *Journal of Fluid Mechanics*, **99**, 13–31.

Dillon T. M. (1982) Vertical overturns: a comparison of Thorpe and Ozmidov length scales. *Journal of Geophysical Research*, **87**, 9601–9613.

Frey H. (1991) A three-dimensional, baroclinic shelf sea circulation model—1. The turbulence closure scheme and the one-dimensional test model. *Continental Shelf Research*, **11**, 365–395.

Galperin B., L. H. Kantha, S. Hassid and A. Rosati (1988) A quasi-equilibrium turbulent energy model for geophysical flows. *Journal of the Atmospherical Sciences*, **45**, 55–62.

Galperin B., A. Rosati, L. H. Kantha and G. L. Mellor (1989) Modeling rotating stratified turbulent flows with application to oceanic mixed layers. *Journal of Physical Oceanography*, **19**, 901–916.

Geernaert G. L., K. B. Katsaros and K. Richter (1986) Variation of the drag coefficient and its dependence on sea state. *Journal of Geophysical Research*, **91**, 7667–7679.

Gesamp (IMO/FAO/UNESCO/WMO/WHO/IAEA/UN/UNEP Joint Group of Experts on the Scientific Aspects of Marine Pollution) (1991) Coastal modelling. GESAMP Reports No. 43, 192 pp.

Gibson M. M. and B. E. Launder (1976) On the calculation of horizontal, turbulent, free shear flows under gravitational influence. *Journal of Heat Transfer*, **C98**, 81–87.

Gibson M. M. and B. E. Launder (1978) Ground effects on pressure fluctuations in the atmospheric boundary layer. *Journal of Fluid Mechanics*, **86**, 491–511.

Gregg M. C. (1987) Diapycnal mixing in the thermocline: a review. *Journal of Geophysical Research*, **92**, 5249–5286.

Heaps N. S. (1972) Estimation of density currents in the Liverpool Bay area of the Irish Sea. *Geophysical Journal of the Royal Astronomical Society*, **30**, 415–432.

Hopfinger E. J. (1987) Turbulence in stratified fluids: a review. *Journal of Geophysical Research*, **92**, 5287–5303.

Hossain M. S. and W. Rodi (1982) A turbulence model for buoyant flows and its application to vertical buoyant jets. In: *Turbulent buoyant jets and plumes*, W. Rodi, editor, HMT Ser., Vol. 6, Pergamon Press, pp. 121–178.

Howard L. N. (1961) Note on a paper of John Miles. *Journal of Fluid Mechanics*, **10**, 509–512.
Itsweire E. C., K. N. Helland and C. W. van Atta (1986) The evolution of a grid-generated turbulence in a stably stratified fluid. *Journal of Fluid Mechanics*, **162**, 299–338.
Johns B., P. Marsaleix, C. Estournel and R. Vehil (1992) On the wind-driven coastal upwelling in the Gulf of Lions. *Journal of Marine Systems*, **3**, 309–320.
Kato H. and O. M. Phillips (1969) On the penetration of a turbulent layer into stratified fluid. *Journal of Fluid Mechanics*, **37**, 643–655.
Kochergin V. P. (1987) Three-dimensional prognostic models. In: *Three-dimensional coastal ocean models, coastal and estuarine sciences 4*, N. S. Heaps, editor, American Geophysical Union, Washington, pp. 201–208.
Kranenburg C. (1983) The influence of side-wall friction on shear-stress driven entrainment experiments. *Journal of Hydraulic Research*, **21**, 99–117.
Kranenburg C. (1984) Wind-induced entrainment in a stably stratified fluid. *Journal of Fluid Mechanics*, **145**, 253–273.
Kundu P. K. (1981) Self-similarity in stress-driven entrainment experiments. *Journal of Geophysical Research*, **86**, 1979–1988.
Kundu P. K. and R. C. Beardsley (1991) Evidence of a critical Richardson number in moored measurements during the upwelling season off Northern California. *Journal of Geophysical Research*, **96**, 4855–4868.
Launder B. E. (1975) On the effects of a gravitational field on the turbulent transport of heat and momentum. *Journal of Fluid Mechanics*, **67**, 569–581.
Launder B. E., G. J. Reece and W. Rodi (1975) Progress in the development of a Reynolds-stress turbulence closure. *Journal of Fluid Mechanics*, **68**, 537–566.
Launder B. E. and D. B. Spalding (1974) The numerical computation of turbulent flows. *Computer Methods in Applied Mechanics and Engineering*, **3**, 269–289.
Mellor G. L. and P. A. Durbin (1975) The structure and dynamics of the ocean surface mixed layer. *Journal of Physical Oceanography*, **5**, 718–728.
Mellor G. L. and H. J. Herring (1973) A survey of mean turbulent field closure models. *AIAA Journal*, **11**, 590–599.
Mellor G. L. and P. T. Strub (1980) Similarity solutions for the stratified turbulent Rayleigh problem. *Journal of Physical Oceanography*, **10**, 455–460.
Mellor G. L. and T. Yamada (1974) A hierarchy of turbulence closure models for planetary boundary layers. *Journal of the Atmospheric Sciences*, **31**, 1791–1806.
Mellor G. L. and T. Yamada (1982) Development of a turbulence closure model for geophysical fluid problems. *Reviews of Geophysics and Space Physics*, **20**, 851–875.
Miles J. W. (1961) On the stability of heterogeneous flows. *Journal of Fluid Mechanics*, **10**, 496–508.
Moum J. N., D. R. Caldwell and C. A. Paulson (1989) Mixing in the equatorial surface layer and thermocline. *Journal of Geophysical Research*, **94**, 2005–2021.
Munk W. H. and E. R. Anderson (1948) Notes on a theory of the thermocline. *Journal of Marine Research*, **7**, 276–295.
Oakey N. S. (1982) Determination of the rate of dissipation of turbulent energy from simultaneous temperature and velocity shear microstructure measurements. *Journal of Physical Oceanography*, **12**, 256–271.
Oey L. and P. Chen (1992) A model simulation of circulation in the Northeast Atlantic Shelves and Seas. *Journal of Geophysical Research*, **97**, 20,087–20,115.
Officer C. B. (1976) *Physical oceanography of estuaries (and associated coastal waters)*. John Wiley, New York, pp. 117–119.
Osborn T. R. (1980) Estimates of the local rate of vertical diffusion from dissipation measurements. *Journal of Physical Oceanography*, **10**, 83–89.
Patankar S. V. (1980) *Numerical heat transfer and fluid flow*. Hemisphere, New York.
Pollard R. T., P. B. Rhines and R. O. R. Y. Thompson (1973) The deepening of the wind-mixed layer. *Geophysical Fluid Dynamics*, **3**, 381–404.
Price J. F. (1979a) On the scaling of stress-driven entrainment experiments. *Journal of Fluid Mechanics*, **90**, 509–529.
Price J. F. (1979b) Observations of a rain-formed mixed layer. *Journal of Physical Oceanography*, **9**, 643–649.
Robert J. L. and Y. Ouellet (1987) A three-dimensional finite element model for the study of steady and non-steady natural flows. In: *Three-dimensional models of marine and estuarine dynamics*, J. C. Nihoul and B. M. Jamart, editors, Elsevier Oceanography Series, Amsterdam, pp. 359–372.

Rodi W. (1984) *Turbulence models and their application in hydraulics*. International Association for Hydraulic Research, 2nd edition, Delft, Netherlands.

Rodi W. (1987) Examples of calculation methods for flow and mixing in stratified fluids. *Journal of Geophysical Research*, **92**, 5305–5328.

Rosati A. and K. Miyakoda (1988) A general circulation model for upper ocean simulation. *Journal of Physical Oceanography*, **18**, 1601–1626.

Ruddick K. G., E. Deleersnijder, T. de Mulder and P. J. Luyten (1994) A model study of the Rhine discharge front and downwelling circulation. *Tellus*, **46A**, 149–159.

Simpson J. H., W. G. Bos, F. Schirmer, A. J. Souza, T. P. Rippeth, S. E. Jones and D. Hydes (1993) Periodic stratification in the Rhine ROFI in the North Sea. *Oceanologica Acta*, **16**, 23–32.

Simpson J. H., J. Brown, J. Matthews and G. Allen (1990) Tidal straining, density currents, and stirring in the control of estuarine stratification. *Estuaries*, **13**, 125–132.

Simpson J. H. and J. R. Hunter (1974) Fronts in the Irish Sea. *Nature*, **250**, 404–406.

Simpson J. H. and J. Sharples (1992) Dynamically active models in the prediciton of estuarine stratification. In: *Dynamics and exchanges in estuaries and the coastal zone, coastal and estuarine studies 40*, D. Prandle, editor, American Geophysical Union, Washington, pp. 101–113.

Simpson J. H., J. Sharples and T. P. Rippeth (1991) A prescriptive model of stratification induced by freshwater runoff. *Estuarine, Coastal and Shelf Science*, **33**, 23–35.

Stillinger D. C., K. N. Helland and C. W. van Atta (1983) Experiments on the transition of homogeneous turbulence to internal waves in a stratified fluid. *Journal of Fluid Mechanics*, **131**, 91–122.

Tennekens H. and J. L. Lumley (1972) *A first course in turbulence*. The MIT Press, Cambridge, pp. 75–95.

Thompson R. O. R. Y. (1979) A reinterpretation of the entrainment process in some laboratory experiments. *Dynamics of Atmospheres and Oceans*, **4**, 45–55.

Trowbridge J. H. (1992) A simple description of the deepening and structure of a stably stratified flow driven by a surface stress. *Journal of Geophysical Research*, **97**, 15,529–15,543.

van der Giessen A., W. P. M. de Ruijter and J. C. Borst (1990) Three dimensional current structure in the Dutch coastal zone. *Netherlands Journal of Sea Research*, **25**, 45–55.

Visser A. W., A. J. Souza, K. Hessner and J. H. Simpson (1994) The effect of stratification on tidal current profiles in a region of freshwater influence. *Oceanologica Acta*, **77**, 369–381.

APPENDIX

Expressions (8) and (9) for the stability coefficients S_u and S_b are derived in the following way. Equations (1) and (5) contain the nine unknown correlations $\langle u_i u_j \rangle$ and $\langle u_i \beta \rangle$. Following the work of Launder (1975), Launder *et al.* (1975), Gibson and Launder (1978) the following modelled transport equations are adopted

$$\frac{\partial}{\partial t}\langle u_i u_j\rangle + U_k \frac{\partial}{\partial x_k}\langle u_i u_j\rangle = -\frac{\partial}{\partial x_k}\langle u_i u_j u_k\rangle + P_{ij} + G_{ij} - c_1 \frac{\varepsilon}{k}\left(\langle u_i u_j\rangle - \frac{2}{3}\delta_{ij}k\right)$$
$$- c_{21}\left(P_{ij} - \frac{2}{3}\delta_{ij}P_s\right) - c_{22}\left(\frac{\partial U_i}{\partial x_j} + \frac{\partial U_j}{\partial x_i}\right)k$$
$$- c_{23}\left(D_{ij} - \frac{2}{3}\delta_{ij}P_s\right) - c_3\left(G_{ij} - \frac{2}{3}\delta_{ij}G\right) - \frac{2}{3}\varepsilon\delta_{ij} \qquad \text{(A1)}$$

$$\frac{\partial}{\partial t}\langle u_i\beta\rangle + U_k\frac{\partial}{\partial x_k}\langle u_i\beta\rangle = -\frac{\partial}{\partial x_k}\langle u_i u_k\beta\rangle - \langle u_i u_k\rangle\frac{\partial b}{\partial x_k}$$
$$- c_{1\beta}\frac{\varepsilon}{k}\langle u_i\beta\rangle + (c_{2\beta} - 1)\left(\langle u_k\beta\rangle\frac{\partial U_i}{\partial x_k} - \delta_{i3}\langle\beta^2\rangle\right) \qquad \text{(A2)}$$

where $k = \Sigma_i \langle u_i^2\rangle/2$ represents the turbulent kinetic energy, ε its dissipation by molecular viscosity and

$$P_{ij} = -\langle u_i u_k\rangle\frac{\partial U_j}{\partial x_k} - \langle u_j u_k\rangle\frac{\partial U_i}{\partial x_k} \qquad \text{(A3)}$$

$$G_{ij} = \delta_{i3}\langle u_j\beta\rangle + \delta_{j3}\langle u_i\beta\rangle \tag{A4}$$

$$D_{ij} = -\langle u_i u_k\rangle \frac{\partial U_k}{\partial x_j} - u_j u_k > \frac{\partial u_k}{\partial z_i} \tag{A5}$$

$$P_s = \frac{1}{2}\sum_i P_{ii}, \qquad G = \frac{1}{2}\sum_i G_{ii} \tag{A6}$$

$$c_{21} = \frac{1}{11}(c_2 + 8), \qquad c_{22} = \frac{1}{55}(30c_2 - 2), \qquad c_{23} = \frac{1}{11}(8c_2 - 2). \tag{A7}$$

The unknown correlation (β^2) which appears in equation (A2) is determined from the transport equation

$$\frac{\partial}{\partial t}\langle\beta^2\rangle + U_k\frac{\partial}{\partial x_k}\langle\beta^2\rangle = -\frac{\partial}{\partial x_k}\langle u_k\beta^2\rangle - 2\langle u_k\beta\rangle\frac{\partial b}{\partial x_k} - \frac{1}{c_{3\beta}}\frac{\varepsilon}{k}\langle\beta^2\rangle. \tag{A8}$$

Launder (1975), Launder *et al.* (1975), Gibson and Launder (1978) determined the empirical constants by reference to laboratory experiments. The following values are adopted:

$$(c_1, c_2, c_3, c_{1\beta}, c_{2\beta}, c_{3\beta}) = (1.5, 0.55, 0.5, 3.0, 0.33, 0.8). \tag{A9}$$

Instead of solving the 10 partial differential equations, together with a separate transport equation for the quantity ε, the problem can be greatly simplified by making the local equilibrium assumption (Mellor and Yamada, 1974, 1982; Hossain and Rodi, 1982). If the time derivative, advective and diffusive transport of the turbulent stresses and fluxes are neglected, the model equations reduce to the following algebraic expressions

$$\begin{aligned}\langle u_i u_j\rangle = {} & \frac{2}{3}\delta_{ij}k + \frac{k}{c_1\varepsilon}\Bigg((1-c_{21})P_{ij} + (1-c_3)G_{ij} \\ & - c_{22}\left(\frac{\partial U_i}{\partial x_j} + \frac{\partial U_j}{\partial x_i}\right)k - c_{23}D_{ij} \\ & + \frac{2}{3}\delta_{ij}((c_{21}+c_{23})P_s + c_3 G - \varepsilon)\Bigg)\end{aligned} \tag{A10}$$

$$\langle u_i\beta\rangle = \frac{1}{c_{1\beta}}\frac{k}{\varepsilon}\left(-\langle u_i u_k\rangle\frac{\partial b}{\partial x_k} + (1-c_{2\beta})\left(d_{i3}\langle\beta^2\rangle - \langle u_k\beta\rangle\frac{\partial U_i}{\partial x_k}\right)\right) \tag{A11}$$

$$\langle\beta^2\rangle = -2c_{3\beta}\frac{k}{\varepsilon}\langle u_k\beta\rangle\frac{\partial b}{\partial x_k}. \tag{A12}$$

In analogy with the level 2.5 model of Mellor and Yamada (1982), the algebraic system (A10)–(A12) is further simplified by using the boundary layer approximation which is justified since the aspect ratio of the flow under consideration is small. This means that vertical hydrostatic equilibrium is assumed and all horizontal derivatives of U and V (horizontal components of the fluid velocity) and b are neglected. The solutions for $\langle uw\rangle$, $\langle vw\rangle$, $\langle w\beta\rangle$ can be written in the form given by equations (6) with ν_T and λ_T given by (7). The algebraic system for the turbulent fluxes then reduces to two linear equations for the stability functions S_u and S_b. The coefficients of those equations are functions of the shear and buoyancy parameters α_M and α_N defined by

$$\alpha_M = \frac{k^2}{\varepsilon^2}(U_z^2 + V_z^2) = \frac{k^2}{\varepsilon^2}M^2, \qquad \alpha_N = \frac{k^2}{\varepsilon^2}b_z = \frac{k^2}{\varepsilon^2}N^2. \tag{A13}$$

Numerical experiments for a wind-driven mixed layer using the analogous Mellor–Yamada formulation performed by Deleersnijder and Luyten (1994) showed that the explicit dependence of the stability functions on shear induces spurious discontinuities in the profiles of velocity and buoyancy. This is related to the observation that the stability parameters are decreasing functions of the shear parameter G_M which is equivalent to α_M in the present notation (Deleersnijder, 1992). Moreover, it appeared that the oscillations are absent when the modified version of Galperin *et al.* (1988) is applied to the Mellor–Yamada level 2.5 model where the shear dependence is eliminated with the aid of the local isotropy approximation. A similar analysis applies to the present case. In analogy with Galperin *et al.* (1988) it can then be shown that S_u and S_b take the form given by equations (8) and (9).